Supplement of Atmos. Meas. Tech., 18, 17–35, 2025
https://doi.org/10.5194/amt-18-17-2025-supplement


Atmospheric Measurement Techniques
Open Access
EGU

*Supplement of*

# Deployment and evaluation of an $NH_4^+$ / $H_3O^+$ reagent ion switching chemical ionization mass spectrometer for the detection of reduced and oxygenated gas-phase organic compounds

**Cort L. Zang and Megan D. Willis**

*Correspondence to:* Megan D. Willis (megan.willis@colostate.edu)

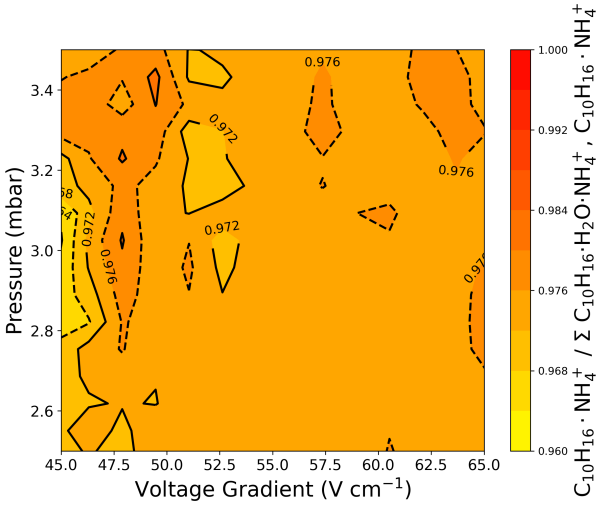


**Figure S1.** Contribution of the $\alpha$-pinene water cluster ($C_{10}H_{16} \cdot H_2O \cdot NH_4^+$) to the sum of the water cluster and molecular ion with $NH_4^+$.

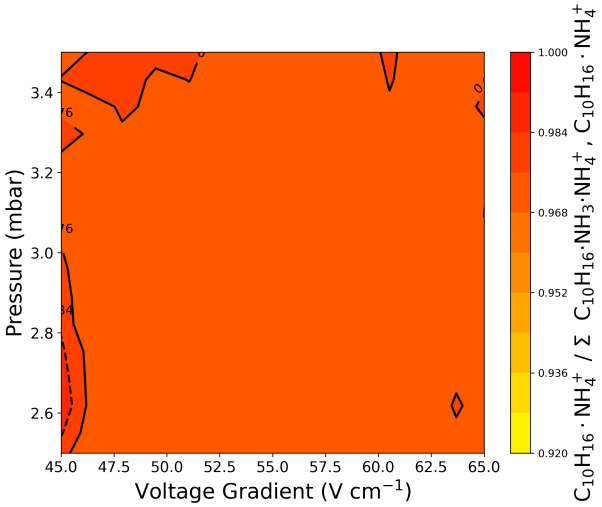


**Figure S2.** Contribution of the $\alpha$-pinene ammonia cluster ($C_{10}H_{16} \cdot NH_3 \cdot NH_4^+$) to the sum of the ammonia cluster and molecular ion with $NH_4^+$.

**Table S1.** Table of instrument voltage settings for different experiments.

| Voltage Name<br>Sections | $NH_4^+$<br>2.2, 2.4, 2.5 | $H_3O^+$<br>2.2, 2.4, 2.5 | $NH_4^+$<br>2.3, 2.6 | $H_3O^+$<br>2.3, 2.6 |
|---|---|---|---|---|
| fIMR Pressure | 3.1 mbar | 2.5 mbar | 3.1 mbar | 2.2 mbar |
| fIMR Temperature | 60.0 C | 60.0 C | 60.0 C | 60.0 C |
| fIMR Front | 650.0 | 650.0 | 600.0 | 675.0 |
| fIMR Back | 0.0 | 30.0 | 0.0 | 50.0 |
| fIMR Amplitude | 450.0 | 450.0 | 500.0 | 500.0 |
| fIMR Frequency | 1.3 MHz | 1.3 MHz | 1.6 MHz | 1.6 MHz |
| Skimmer 1 | -4.9 | -4.7 | -6.0 | -5.9 |
| BSQ Front | -10.2 | -10.2 | -10.7 | -9.7 |
| BSQ Back | -11.4 | -12.7 | -11.9 | -13.9 |
| BSQ Amplitude | 250.0 | 350.0 | 250.0 | 270.0 |
| BSQ Frequency | 2.2 MHz | 2.2 MHz | 2.2 MHz | 2.2 MHz |
| Skimmer 2 | *See Trans A/B* | *See Trans A/B* | *See Trans A/B* | *See Trans A/B* |
| Trans A | -10.8 | -11.0 | -10.8 | -11.0 |
| Trans B | -13.0 | -13.0 | -13.0 | -13.0 |
| Ion Lens 2 | -74.3 | -62.6 | -71.8 | -69.8 |
| Deflector Flange | -93.1 | -95.9 | -97.9 | -93.7 |
| Deflector | -103.2 | -107.3 | -106.4 | -103.9 |
| Reference | -140.0 | -110.1 | -148.0 | -136.0 |

Values in table are reported in volts unless otherwise noted.

**Table S2.** Standardized gas cylinders and the composition.

| Tank 1 Component | Conc. (ppb) | Tank 2 Component | Conc. (ppb) | Tank 3 Component | Conc. (ppb) |
|---|---|---|---|---|---|
| Methane thiol | 986 | Acetonitrile | 1012 | Acetaldehyde | 1003 |
| Isoprene | 1005 | Dimethyl sulfide | 998 | Acetone | 1058 |
| Hydroxyacetone | 984 | Methyl Vinyl Ketone | 1046 | Methyl Ethyl Ketone | 1050 |
| Dimethyl sulfoxide | 992 | Benzene | 1023 | Toluene | 1009 |
| trans-2-hexenal | 967 | 1-Methoxy-2-propanol | 1090 | trans-3-hexenol | 990 |
| Phenol | 471 | 3-Hexanone | 980 | 2-Octanone | 975 |
| 1,3,5-Trimethylbenzene | 991 | Limonene | 981 | Camphor | 980 |
| beta-Cylcocitral | 916 | beta-Ionone | 327 | D5-Siloxane | 937 |

**Table S3.** Table of $NH_4^+$ and $H^+$ affinities obtained from the NIST Chemistry WebBook (Edward P. Hunter and Sharon G. Lias; Michael M. Meot-Ner (Mautner) and Sharon G. Lias).

| Compound | $NH_4^+$ Affinity [kJ $mol^{-1}$] | $H^+$ Affinity [kJ $mol^{-1}$] |
|---|---|---|
| Ethylene | 42 | 681 |
| Acetone | 118 | 812 |
| Methylal | 122 | *no data* |
| 2-Methyl-propene | 146 | 802 |
| 1,2-Dimethoxy-ethane | 160 | 858 |
| Benzene | 81 | 750 |
| Cyclohexane | 40 | 687 |
| 1,3,5-Trimethylbenzene | 91 | 836 |
| Hydrogen sulfide | 48 | 705 |
| Water | 86 | 691 |
| Ammonia | 107 | 854 |

**Table S4.** Vapor pressure estimates of certified gas standard analytes at 25°C.[a]

| Analyte | Formula | Vapor Pressure $\mu$g m$^{-3}$ | Vapor Pressure Pa | Method |
|---|---|---|---|---|
| dimethyl sulfide | $C_2H_6S$ | 1.60E+9 | 6.38E+4 | Mean VP of Antoine & Grain methods |
| methane thiol | $CH_4S$ | 3.92E+9 | 2.02E+5 | Mean VP of Antoine & Grain methods |
| dimethyl sulfoxide | $C_2H_6SO$ | 2.61E+6 | 82.9 | Mean VP of Antoine & Grain methods |
| benzene | $C_6H_6$ | 3.66E+8 | 1.16E+4 | Mean VP of Antoine & Grain methods |
| toluene | $C_7H_8$ | 1.17E+8 | 3.16E+3 | Mean VP of Antoine & Grain methods |
| 1,3,5-trimethylbenzene | $C_9H_{12}$ | 1.30E+7 | 268 | Mean VP of Antoine & Grain methods |
| phenol | $C_6H_6O$ | 1.63E+6 | 43 | Modified Grain method |
| isoprene | $C_5H_8$ | 2.02E+9 | 7.35E+4 | Mean VP of Antoine & Grain methods |
| limonene | $C_{10}H_{16}$ | 1.06E+7 | 193 | Mean VP of Antoine & Grain methods |
| acetone | $C_3H_6O$ | 7.78E+8 | 3.32E+4 | Mean VP of Antoine & Grain methods |
| hydroxyacetone | $C_3H_6O_2$ | 6.93E+6 | 232 | Mean VP of Antoine & Grain methods |
| methyl ethyl ketone | $C_4H_8O$ | 3.81E+8 | 1.31E+4 | Mean VP of Antoine & Grain methods |
| methyl vinyl ketone | $C_4H_6O$ | 3.45E+8 | 1.22E+4 | Mean VP of Antoine & Grain methods |
| 3-hexanone | $C_6H_{12}O$ | 8.73E+7 | 2.16E+3 | Mean VP of Antoine & Grain methods |
| 2-octanone | $C_8H_{16}O$ | 1.27E+7 | 246 | Mean VP of Antoine & Grain methods |
| camphor | $C_{10}H_{16}O$ | 8.72E+4 | 1.42 | Modified Grain method |
| acetaldehyde | $C_2H_4O$ | 2.15E+9 | 1.21E+5 | Mean VP of Antoine & Grain methods |
| trans-2-hexenal | $C_6H_{10}O$ | 2.49E+7 | 629 | Mean VP of Antoine & Grain methods |
| beta-cyclocitral | $C_{10}H_{16}O$ | 1.48E+6 | 24.1 | Mean VP of Antoine & Grain methods |
| trans-3-hexenol | $C_6H_{12}O$ | 5.05E+6 | 125 | Mean VP of Antoine & Grain methods |
| acetonitrile | $C_2H_3N$ | 4.42E+8 | 2.67E+4 | Mean VP of Antoine & Grain methods |
| 1-methoxy-2-propanol | $C_4H_{10}O_2$ | 3.58E+7 | 984 | Mean VP of Antoine & Grain methods |
| D5-Siloxane | $C_{10}H_{30}O_5Si_5$ | 4.35E+6 | 29.1 | Mean VP of Antoine & Grain methods |

[a] Estimated using EPI Suite (US EPA).

**Table S5.** Comparison of sensitivities with $NH_4^+$ ionization calculated in this study with those reported by Xu et al. (2022).[a]

| Analyte | This Study counts $s^{-1}$ $ppt_v^{-1}$ | Xu et al. (2022) counts $s^{-1}$ $ppt_v^{-1}$ |
|---|---|---|
| Acetonitrile | 0.85 | 0.55 |
| Acetaldehyde | <0.1 | 0.021 |
| Acetone | 0.98 | 1.2 |
| Isoprene | <0.1 | 0.028 |
| Methyl vinyl ketone | 1.5 | 1.5 |
| Methyl ethyl ketone | 1.3 | 1.6 |
| Hydroxyacetone | 1.6 | 2.1 |
| Benzene | <0.1 | <0.001 |
| Phenol | <0.1 | 0.19 |
| Hexanone[b] | 3.4 | 3.8 |
| Trimethylbenzene | <0.1 | <0.001 |

[a] We are using a Vocus-S and Xu et al. (2022) report using a Vocus-2R which have different time-of-flight region lengths. The instruments also differ in extraction frequency (i.e., 25 kHz here, and 17.5 kHz for Xu et al. (2022)).

[b] This study used 3-Hexanone and Xu et al. (2022) used 2-Hexanone.

**Table S6.** Fractional signal contributions for Fig. 3 with $H_3O^+$ in the top half and $NH_4^+$ in the bottom half.

| $H_3O^+$ ionization | 2-hexanone | trans-2-hexen-1-ol | 2-methyl-3-butene-2-ol | trans-2-hexenal | beta-cyclocitral |
|---|---|---|---|---|---|
| $A \cdot H^+$ | 0.67 | 0.00 | 0.19 | 0.44 | 0.58 |
| $A \cdot H^+$-$H_2O$ | 0.13 | 0.78 | 0.77 | 0.47 | *n.o.* |
| $A \cdot H^+$-$H_2O$, $H_2$ | *n.o.* | 0.09 | 0.03 | *n.o.* | *n.o.* |
| $A \cdot H^+$-$H_2O$, $CH_4$ | *n.o.* | 0.06 | *n.o.* | *n.o.* | *n.o.* |
| $A \cdot H^+$-$H_2$ | *n.o.* | 0.06 | *n.o.* | *n.o.* | *n.o.* |
| $A \cdot H^+$-$H_2CO$ | *n.o.* | *n.o.* | *n.o.* | 0.09 | 0.12 |
| $A \cdot H^+$-$C_xH_{2x}O$ | *n.o.* | *n.o.* | *n.o.* | *n.o.* | 0.29 |
| $A \cdot H^+ \cdot H_2O$ | 0.20 | *n.o.* | *n.o.* | *n.o.* | *n.o.* |
| $NH_4^+$ ionization | - | - | - | - | - |
| $A \cdot NH_4^+$ | 0.95 | 0.66 | 0.31 | 0.95 | 0.94 |
| $A \cdot NH_4^+$-$H_2O$ | *n.o.* | 0.08 | 0.68 | *n.o.* | *n.o.* |
| $A \cdot NH_4^+$-$H_2$ | *n.o.* | 0.21 | 0.03 | *n.o.* | *n.o.* |
| $A \cdot NH_4^+$-$H_2CO$ | *n.o.* | *n.o.* | *n.o.* | *n.o.* | 0.01 |
| $A \cdot NH_4^+$-$CH_4$ | *n.o.* | 0.02 | *n.o.* | *n.o.* | *n.o.* |
| $A \cdot H^+$ | *n.o.* | *n.o.* | *n.o.* | *n.o.* | 0.02 |
| $A \cdot NH_4^+ \cdot NH_3$ | 0.02 | 0.01 | 0.00 | 0.02 | 0.01 |
| $A \cdot NH_4^+ \cdot H_2O$ | 0.03 | 0.02 | 0.01 | 0.03 | 0.01 |

Values in the table are the fractional contributions of various fragments, clusters, or the molecular ions. If a fragment or cluster is not observed for an analyte is it noted as *n.o.* (not observed).

**Table S7.** Vapor pressure estimates of potential biogenic ROC analytes at 25°C.[a]

| Analyte<br>*MCM name* | Formula | Vapor Pressure<br>$\mu$g m$^{-3}$ | Vapor Pressure<br>Pa | Method |
|---|---|---|---|---|
| LIMCOOH | $C_{10}H_{18}O_3$ | 4.40E+2 | 0.00586 | Modified Grain method |
| LIMAOH | $C_{10}H_{18}O_2$ | 3.55E+3 | 0.0517 | Modified Grain method |
| LIMBCO | $C_{10}H_{16}O_2$ | 7.47E+3 | 0.11 | Modified Grain method |
| LIMONONIC | $C_{10}H_{16}O_3$ | 8.77E+3 | 0.118 | Modified Grain method |
| APINBCO | $C_{10}H_{16}O_2$ | 1.76E+4 | 0.26 | Modified Grain method |
| PINAL | $C_{10}H_{16}O_2$ | 3.62E+5 | 5.34 | Modified Grain method |
| PINONIC | $C_{10}H_{16}O_3$ | 6.15E+3 | 0.0828 | Modified Grain method |
| C109OH | $C_{10}H_{16}O_3$ | 4.66E+2 | 0.00627 | Modified Grain method |
| C107OH | $C_{10}H_{16}O_3$ | 1.99E+3 | 0.0268 | Modified Grain method |
| HCOC5 | $C_5H_8O_2$ | 2.07E+6 | 51.2 | Mean VP of Antoine & Grain methods |
| LIMALNO3 | $C_{10}H_{17}NO_6$ | 1.16E+1 | 0.000116 | Modified Grain method |
| NLIMALOH | $C_{10}H_{17}NO_6$ | 2.32E+1 | 0.000233 | Modified Grain method |
| MBOANO3 | $C_5H_{11}NO_5$ | 7.79E+3 | 0.117 | Modified Grain method |

[a] Estimated using EPI Suite (US EPA).

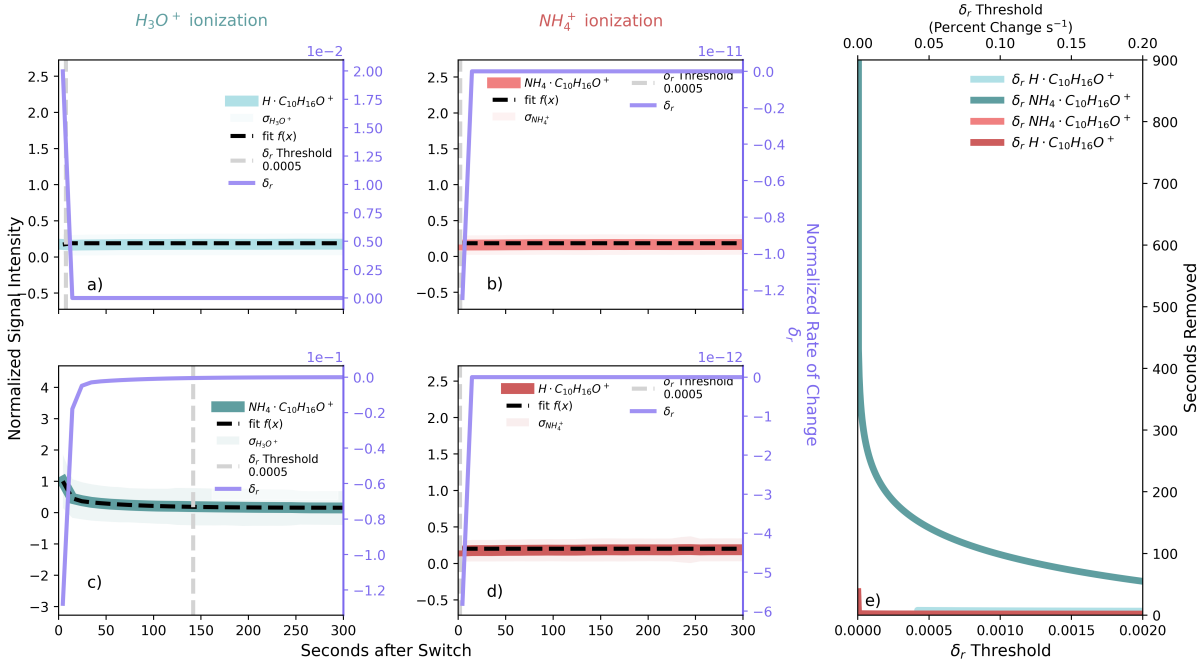


**Figure S3.** Ion signal after a reagent-ion switch for $H_3O^+$ (a & c) and $NH_4^+$ (b & d) to the $C_{10}H_{16}O \cdot H^+$ (a & d) and $C_{10}H_{16}O \cdot NH_4^+$ (b & c), in the MEFO observations. We grouped ion signals by the time after a switch and normalized the mean of each group by the maximum, and normalized means were fit with a bi-exponential function. The derivative of the fit ($\delta_n$) is displayed on the right axes for (a-d) and used as a metric to filter reagent-ion hysteresis. (e) The number of seconds removed after a switch as a function of $\delta_n$ threshold for various ions.

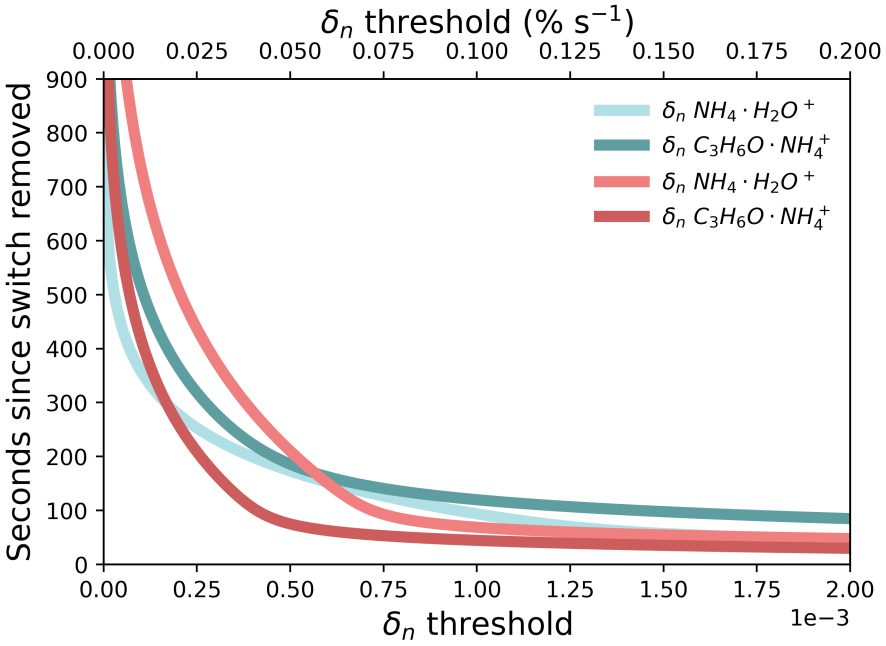


**Figure S4.** The number of seconds removed after a switch as a function of $\delta_n$ threshold for various ions, in the MEFO observations.

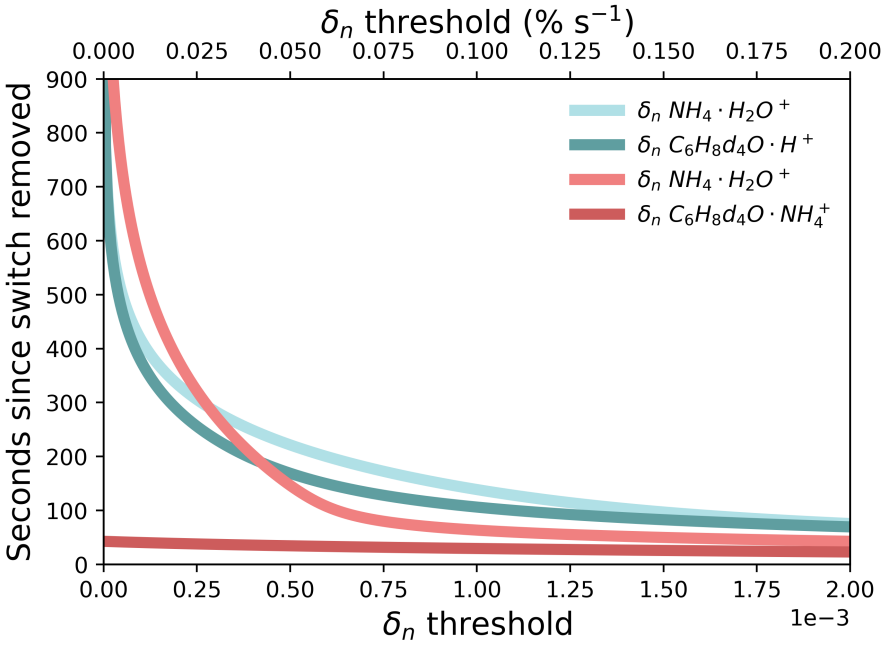


**Figure S5.** The number of seconds removed after a switch as a function of $\delta_n$ threshold for various ions, in the ARTofMELT observations.

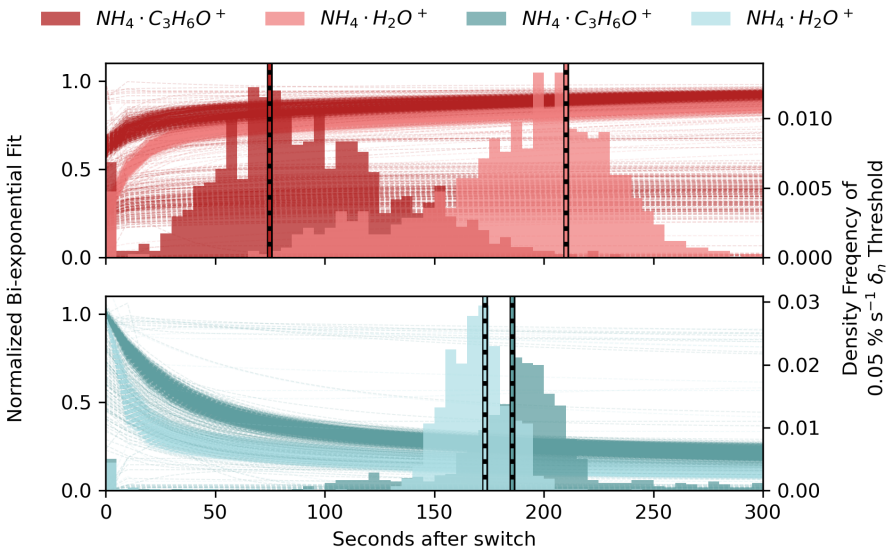


**Figure S6.** Traces of bi-exponential fit for individual switches with $NH_4^+$ ionization (top) and $H_3O^+$ ionization (bottom) as well as a histogram of the time at which a 0.05 % $s^{-1}$ change threshold is reached across individual switches. Dashed lines with black background show the cutoff from the average analysis used in Sect. 3.4. Data is from the MEFO.

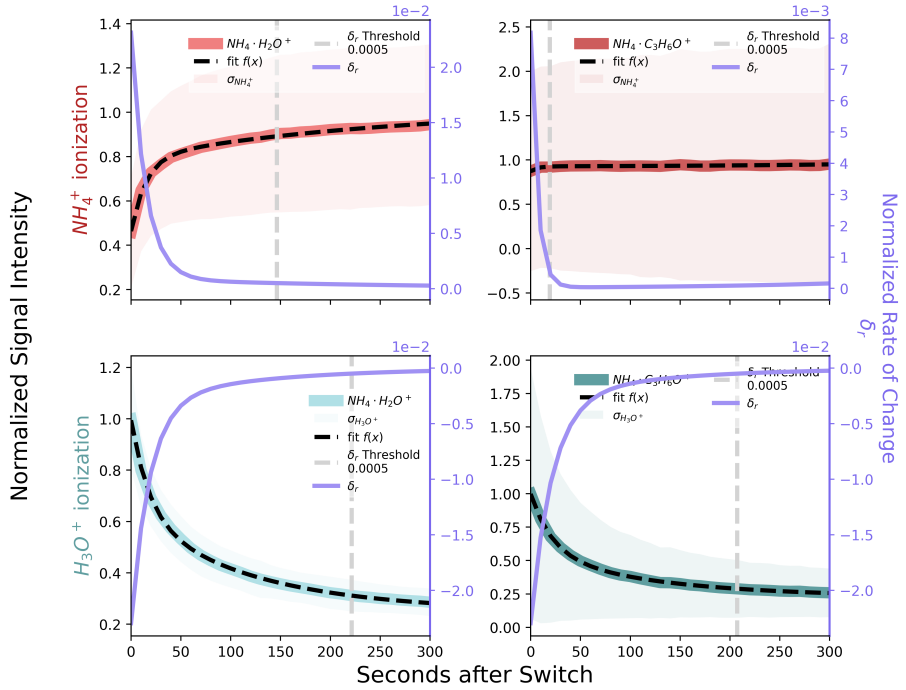


**Figure S7.** Ion signal after a reagent-ion switch for $NH_4^+$ (top, orange) and $H_3O^+$ (bottom, blue) in the ARTofMELT data, showing $NH_4 \cdot H_2O^+$ ions (left) and $C_3H_6O \cdot NH_4^+$ (right) ambient analyte ions. We grouped ion signals by the time after a switch and normalized the mean of each group by the maximum, and normalized means were fit with a bi-exponential function. The derivative of the fit ($\delta_n$) is displayed on the right axes (purple traces) and is used as a metric to filter reagent-ion hysteresis.

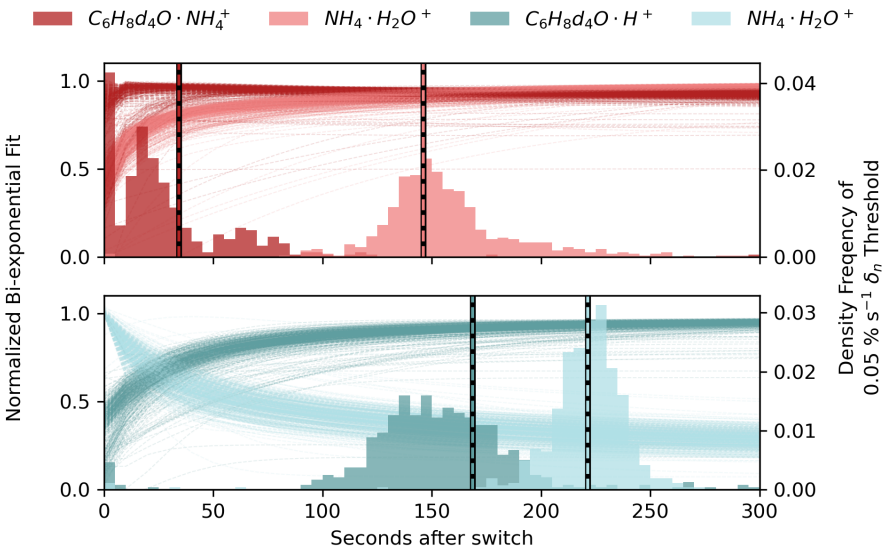


**Figure S8.** Traces of bi-exponential fit for individual switches with $NH_4^+$ ionization (top) and $H_3O^+$ ionization (bottom) as well as a histogram of the time at which a 0.05 % $s^{-1}$ change threshold is reached across individual switches. Dashed lines with black background show the cutoff from the average analysis used in Sect. 3.4. Data is from a 2-week period of the ARTofMELT expedition.

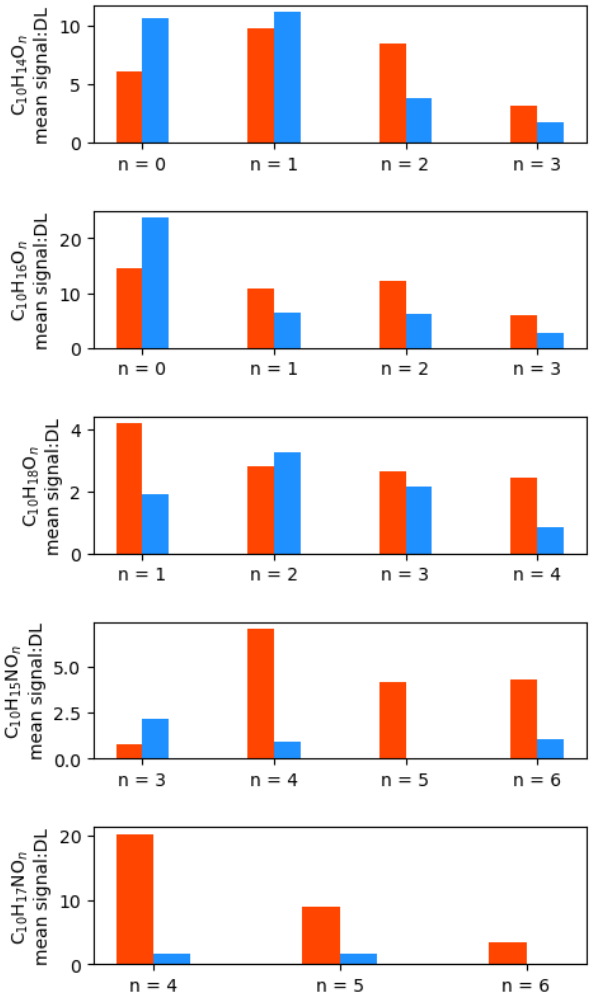


**Figure S9.** Bar chart comparison of the signal-to-DL ratio for various selected ions from Fig. 7 of the main text. Ions detected with $NH_4^+$ are displayed as orange, and ions detected with $H_3O^+$ are displayed as blue.

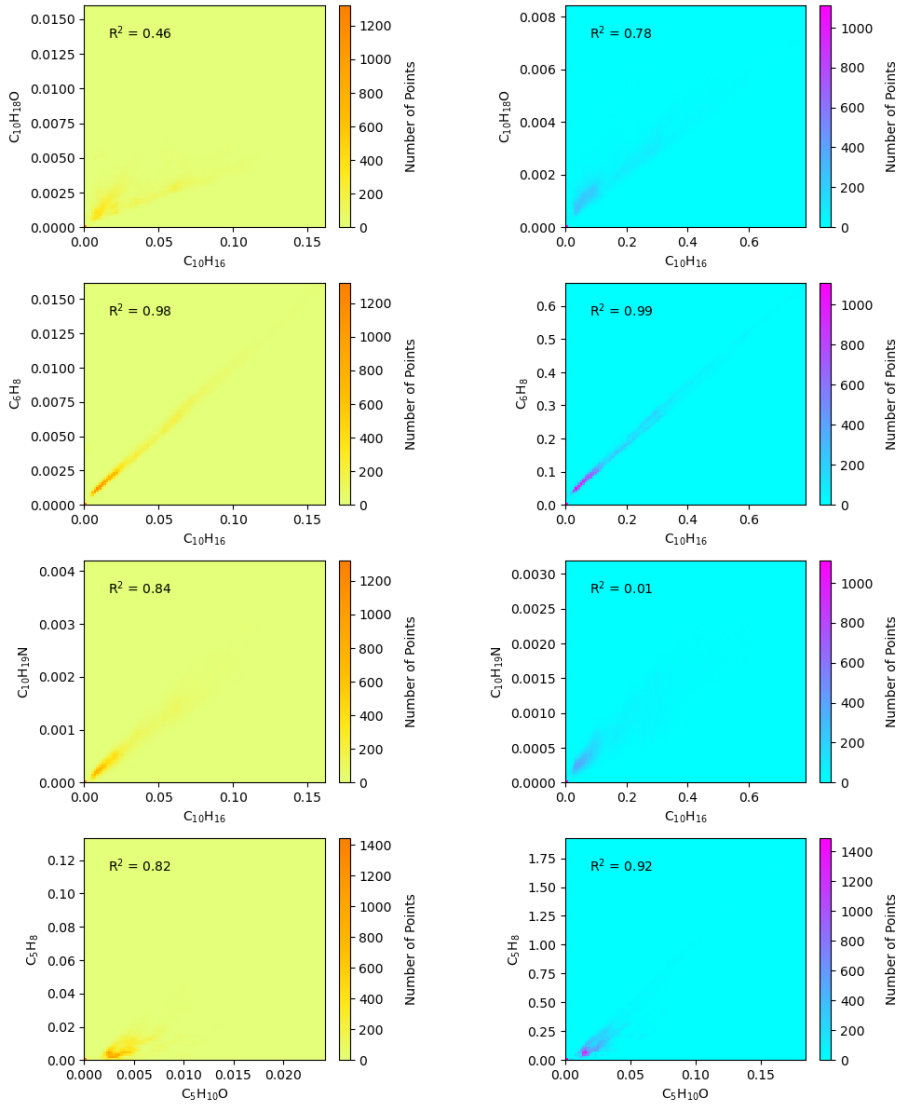


**Figure S10.** 2D-histograms of ion signals for a selection of ions detected by $NH_4^+$ (orange/yellow, left) and $H_3O^+$ (blue/purple, right). Color bars show frequency per bin for the 100 x100 bin grid. Signals for the ions are in counts extraction$^{-1}$ at 25 kHz extraction frequency.

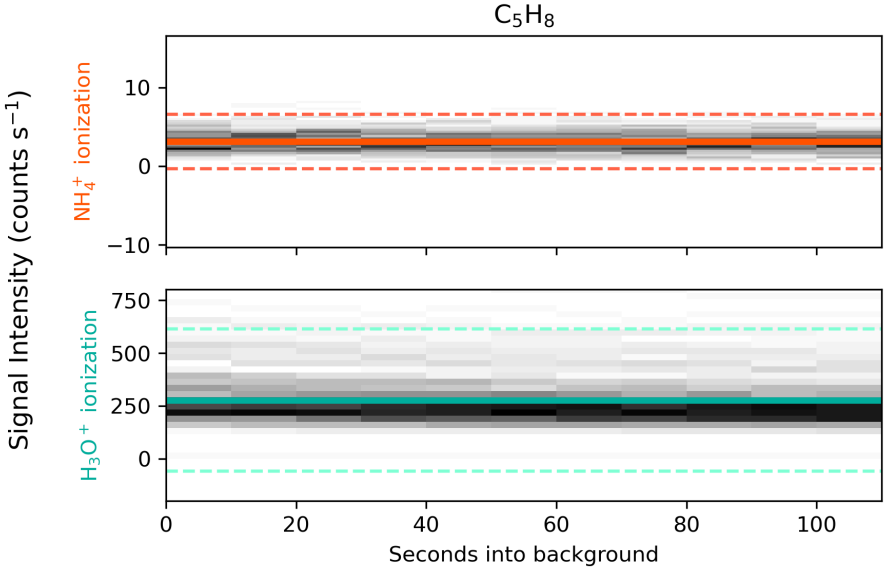


**Figure S11.** 2D-histograms of campaign zero periods for the $C_5H_8$ ion detected with $NH_4^+$ (orange, top) and $H_3O^+$ (blue, bottom). Solid horizontal lines represent mean signal during zero periods and dashed lines represent 3 $\sigma$ deviation from the mean.

**Table S8.** Potential structures and literature precedent for organic nitrate peaks.

| Chemical Formula | Name in MCM[a] | Reported in Fry et al. (2013)? | Potential Assignment |
|---|---|---|---|
| $C_5H_9NO_5$ | NMBOBCO<br>C4MCONO3OH | no | 232-MBO nitrate/ Isoprene nitrate |
| $C_5H_{11}NO_5$ | MBOANO3 | no | 232-MBO nitrate |
| $C_{10}H_{15}NO_3$ | | no | Dehydration fragment of $C_{10}H_{17}NO_4$ |
| $C_{10}H_{15}NO_4$ | NC101CO<br>NC91CHO | yes (night) | Terpene nitrate (carbonyl) |
| $C_{10}H_{15}NO_5$ | PINALNO3 | no | Fragment from LIMALNO3?<br>Faxon et al. (2018) speculate that is could be a fragment of dimers.<br>Oxidation of primary emissions of terpenoid oxygenates. |
| $C_{10}H_{15}NO_6$ | C10PAN2<br>C923PAN<br>C918PAN<br>C108NO3 | no | Terpene nitrate (PAN/carbonyl nitrate) |
| $C_{10}H_{17}NO_4$ | APINCNO3<br>BPINBNO3<br>LIMANO3<br>LIMCNO3<br>APINANO3<br>BPINANO3 | yes (day and night) | Terpene nitrate (alcohol) |
| $C_{10}H_{17}NO_5$ | NBPINAOOH<br>NAPINBOOH<br>NLIMOOH | yes (night) | Terpene nitrate (hydroperoxy) |
| $C_{10}H_{17}NO_6$ | LIMALNO3<br>NLIMALOH | no | Limonene nitrate |
| $C_{10}H_{16}N_2O_6$ | | no | Proposed as $\alpha$-pinene oxidation product (Bates et al., 2022) |

[a]Exploration of the MCM is non-exhaustive (Saunders et al., 2003; Jenkin et al., 2015).

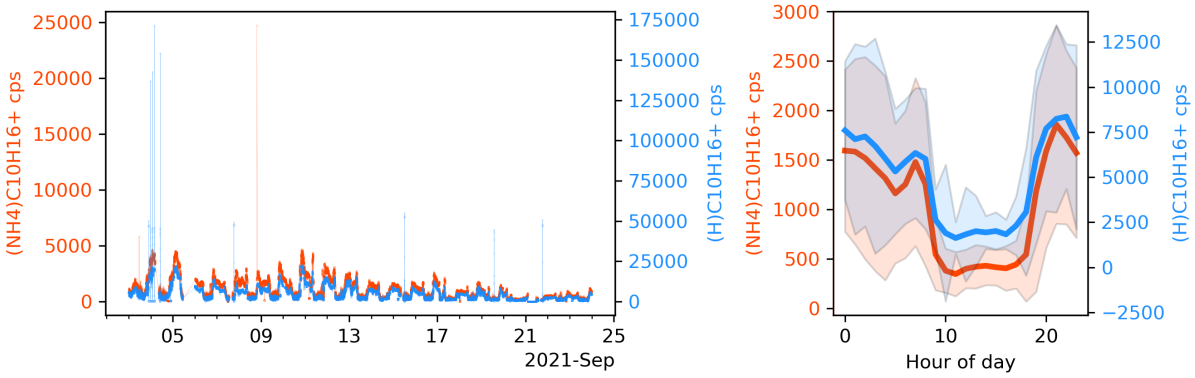


**Figure S12.** Time-series of ion signals of $NH_4^+ \cdot C_{10}H_{16}$ detected by $NH_4^+$ (orange) and $H^+ \cdot C_{10}H_{16}$ $H_3O^+$ (blue). Diurnal averages are included in the right plot.

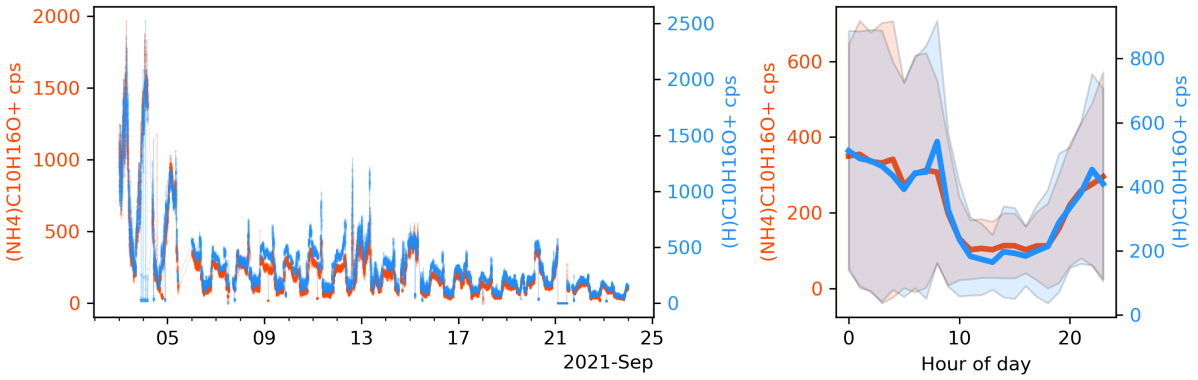


**Figure S13.** Time-series of ion signals of $NH_4^+ \cdot C_{10}H_{16}O$ detected by $NH_4^+$ (orange) and $H^+ \cdot C_{10}H_{16}O\ H_3O^+$ (blue). Diurnal averages are included in the right plot.

## References


Bates, K. H., Burke, G. J. P., Cope, J. D., and Nguyen, T. B.: Secondary organic aerosol and organic nitrogen yields from the nitrate radical (NO3) oxidation of alpha-pinene from various RO2 fates, Atmospheric Chemistry and Physics, 22, 1467–1482, https://doi.org/10.5194/acp-22-1467-2022, 2022.

Edward P. Hunter and Sharon G. Lias: Proton Affinity Evaluation, in: NIST Chemistry WebBook, NIST Standard Refernce Database Number 69, Eds. P.J. Linstrom and W.G. Mallard, National Institude of Standards and Technology, Gaithersburg MD, 20899, https://doi.org/https://doi.org/10.18434/T4D303.

Faxon, C., Hammes, J., Le Breton, M., Pathak, R. K., and Hallquist, M.: Characterization of organic nitrate constituents of secondary organic aerosol (SOA) from nitrate-radical-initiated oxidation of limonene using high-resolution chemical ionization mass spectrometry, Atmospheric Chemistry and Physics, 18, 5467–5481, https://doi.org/10.5194/acp-18-5467-2018, 2018.

Fry, J. L., Draper, D. C., Zarzana, K. J., Campuzano-Jost, P., Day, D. A., Jimenez, J. L., Brown, S. S., Cohen, R. C., Kaser, L., Hansel, A., Cappellin, L., Karl, T., Hodzic Roux, A., Turnipseed, A., Cantrell, C., Lefer, B. L., and Grossberg, N.: Observations of gas- and aerosol-phase organic nitrates at BEACHON-RoMBAS 2011, Atmospheric Chemistry and Physics, 13, 8585–8605, https://doi.org/10.5194/acp-13-8585-2013, 2013.

Jenkin, M. E., Young, J. C., and Rickard, A. R.: The MCM v3.3.1 degradation scheme for isoprene, Atmospheric Chemistry and Physics, 15, 11 433–11 459, https://doi.org/10.5194/acp-15-11433-2015, 2015.

Michael M. Meot-Ner (Mautner) and Sharon G. Lias: Binding Energies Between Ions and Molecules, and The Thermochemistry of Cluster Ions, in: NIST Chemistry WebBook, NIST Standard Reference Database Number 69, Eds. P.J. Linstrom and W.G. Mallard, National Institude of Standards and Technology, Gaithersburg MD, 20899, https://doi.org/https://doi.org/10.18434/T4D303.

Saunders, S. M., Jenkin, M. E., Derwent, R. G., and Pilling, M. J.: Protocol for the development of the Master Chemical Mechanism, MCM v3 (Part A): tropospheric degradation of non-aromatic volatile organic compounds, Atmospheric Chemistry and Physics, 3, 161–180, https://doi.org/10.5194/acp-3-161-2003, 2003.

US EPA: Estimations Programs Interface Suite for Microsoft Windows, https://www.epa.gov/tsca-screening-tools/epi-suitetm-estimation-program-interface.

Xu, L., Coggon, M. M., Stockwell, C. E., Gilman, J. B., Robinson, M. A., Breitenlechner, M., Lamplugh, A., Crounse, J. D., Wennberg, P. O., Neuman, J. A., Novak, G. A., Veres, P. R., Brown, S. S., and Warneke, C.: Chemical ionization mass spectrometry utilizing ammonium ions ($NH_4^+$ CIMS) for measurements of organic compounds in the atmosphere, Atmospheric Measurement Techniques, 15, 7353–7373, https://doi.org/10.5194/amt-15-7353-2022, 2022.